Provided for non-commercial research and education use.
Not for reproduction, distribution or commercial use.

This article appeared in a journal published by Elsevier. The attached copy is furnished to the author for internal non-commercial research and education use, including for instruction at the authors institution and sharing with colleagues.

Other uses, including reproduction and distribution, or selling or licensing copies, or posting to personal, institutional or third party websites are prohibited.

In most cases authors are permitted to post their version of the article (e.g. in Word or Tex form) to their personal website or institutional repository. Authors requiring further information regarding Elsevier's archiving and manuscript policies are encouraged to visit:

http://www.elsevier.com/copyright

Author's personal copy

Thin Solid Films 520 (2012) 4254–4258

Contents lists available at SciVerse ScienceDirect

Thin Solid Films

journal homepage: www.elsevier.com/locate/tsf

Structural properties of porous silicon/SnO_2:F heterostructures

F.A. Garcés [a,*], L.N. Acquaroli [a], R. Urteaga [a,b], A. Dussan [c], R.R. Koropecki [a,b], R.D. Arce [a,b]

[a] Instituto de Desarrollo Tecnológico para la Industria Química, UNL-CONICET, Güemes 3450, S3000GLN Santa Fe, Argentina
[b] Facultad de Ingeniería Química, UNL, Santiago del Estero 2829, S3000AOM Santa Fe, Argentina
[c] Grupo de Materiales Nanoestructurados y sus Aplicaciones, Universidad Nacional de Colombia, Colombia

ARTICLE INFO

Article history:
Received 8 June 2011
Received in revised form 27 January 2012
Accepted 2 February 2012
Available online 10 February 2012

Keywords:
Porous silicon
Transparent conducting oxides
Sol–gel deposition
Tin oxide
Doped oxides
Microstructure
X-ray diffraction

ABSTRACT

In this work we present structural studies made on SnO_2 deposited on macroporous silicon structures. The porous silicon substrates were prepared by anodization of p-type silicon wafers. The SnO_2 doped layers were synthesized by the sol–gel method from $SnCl_4 \cdot 5H_2O$-ethanolic precursor, where the effect of fluorine doping level on structural properties was investigated. The fundamental structural parameters of tin oxide such as the lattice parameter and the crystallite size were studied in correlation with the dopant concentration. In addition, the effect of fluorine incorporation into the structure of tin oxide was analyzed on the basis of theoretical calculations that take into account the structural factor. The results obtained indicate that incorporation of fluorine occurs only at substitutional sites for SnO_2 deposited on porous silicon.

© 2012 Elsevier B.V. All rights reserved.

1. Introduction

Heterostructures formed by porous silicon (PS) and transparent conductive oxide (TCO), such as SnO_2 have been of great interest in recent years. The interest lies in a wide range of properties of these junctions such as light emission [1], the realization of electrical contacts in the volume of the porous film improved the electroluminescence efficiency [2], and implementation of structures with particular sensing properties [3].

The aggregates used in these oxides tend to act as dopant. Typical dopants in the case of SnO_2 may be F, Cl, or Sb. The inclusion of these dopants in SnO_2 alters the original oxide properties [4], not only those related to the electronic transport, but also modifying the structural properties like the lattice parameter. Various authors have discussed the influence of the doping level on structural, electrical and optical properties when the oxide is deposited onto flat substrates [5–8]. Oshima et al. found that some orientations are prominent with increasing of fluorine concentration [9]. The same authors also report that fluorine doping causes the degree of crystallinity of the SnO_2 films to increase. On the other hand, theoretical calculations made by Vienna Ab-Initio Simulation Package have determined that fluorine ions occupy the corresponding oxygen sites in the crystal lattice [10], and F doping produces a decrease in the resistivity [5,10].

The synthesis of SnO_2 can be done by a variety of methods, among them: Chemical Vapor Deposition [11], reactive sputtering [12], and spray pyrolysis [13]. These techniques allow the growth of materials in the form of thin films with a high degree of homogeneity. Nevertheless, the application of these techniques to the insertion of conductive oxide like SnO_2 into a PS matrix does not provide good homogeneity in composition; even more, the coverage is not complete [14].

Sol–gel synthesis [15] has recently gained great interest for the manufacture of materials based on metal oxides like SnO_2, which can be attributed to several advantages: easily adjust of proportion of the compounds of interest, simple and cheap implementation of the equipment, and mostly, the process is done at a relatively low temperature.

In this paper we show results obtained for SnO_2/PS heterostructures synthesized by sol–gel method. Good filling of the porous structure was achieved by functionalizing appropriately the PS macrostructure. The process reduces the hydrophobicity of its surface, and allows the SnO_2 precursors to penetrate deeply into the PS pores.

The effects of fluorine doping on SnO_2 were analyzed within the frame of a theoretical model, which can be used to identify possible routes for the occupation of lattice sites by fluorine ions. Characterization techniques, such as scanning electronic microscopy, infrared transmittance and X-ray diffraction, were used in order to get insight of the structural behavior of the layers. The role of doping effect on tin oxide structure and PS surface modification is discussed as well.

2. Experimental details

Porous silicon layers were obtained by electrochemical anodization of p-type boron doped crystalline silicon wafers, orientation

* Corresponding author. Fax: +54 342 4550944.
E-mail address: fgarces@intec.unl.edu.ar (F.A. Garcés).

0040-6090/$ – see front matter © 2012 Elsevier B.V. All rights reserved.
doi:10.1016/j.tsf.2012.02.009

Author's personal copy

(100) and resistivity 25.5–42.5 Ω-cm, in a hydrofluoric acid 49.9% and N,N dimethylformamide electrolyte solution in proportions 1:9 in volume. The galvanostatic process was carried for 900 s using a 10 mA/cm^2 current density in darkness. The process is carried out in a Teflon beaker with platinum wire electrode as the cathode and the silicon wafer as the anode. Aluminum 99.99% was evaporated as a backside contact of the Si wafer to improve the distribution of the current density in the anodization stage. With this procedure we obtained the p-type region of the heterojunction. The n-type region was fabricated synthesizing fluorine doped tin oxide by the sol gel method [13]. SnO_2 and SnO_2:F solutions were deposited onto PS layers by chemical bath and dip coating procedures. Previously, porous surface was functionalized with tetra-butyl hydroxide ammonia (TBHA) 1% during 10 min in an ultrasonic bath. This treatment removes hydrophobic effects in PS caused by hydrogen termination [16]. Precursor solutions were obtained by adding different proportions of NH_4F dissolved in ethyl alcohol to a 0.042 M ethanolic $SnCl_4 \cdot 5H_2O$ solution [17]. The NH_4F concentrations in the solution ranged from 0% to 14%. These solutions were maintained at 65 °C during 60 min until metal hydroxylation takes place. For the TCO deposition onto PS, we used a chemical bath temperature of 65 °C, and the homogenization of the gel thickness on PS was achieve with a spinner system rotating at 3000 rpm. Then, the samples were heated at 65 °C to eliminate residual solvents. These parameters were kept constant for all prepared samples. Once the residual solvent was eliminated, a thermal annealing was performed in a rapid thermal annealing furnace (RTA) at atmospheric pressure, to obtain a condensed tin oxide structure [1,18]. The RTA thermal ramp executed was as follows: (i) 10 min. at 400 °C (Pre-condensation structure), (ii) 10 min. at 550 °C (Crystallization). The heating rate between the steps was kept at 5 °C/min in all cases.

All layers were characterized by means of X-ray diffraction measurements, scanning electron microscopy (SEM) and infrared transmittance spectroscopy (IR). X-ray diffraction was carried out on a Panalytical X'Pert PRO MPD diffractometer operating with λ:1.541 Å Cu Kα radiation in a θ–2θ drive configuration; SEM images were obtained in a scanning electronic microscope JEOL J5M-35C. The images were taken operating the microscope at 20 kV, while infrared transmittance spectra were measured with a NIKOLET 8700 FTIR in a range of measurement from 400 cm^{-1} to 4000 cm^{-1}, performing an average over 100 spectra.

3. Results and discussion

Fig. 1 shows SEM images of two similar samples, (Fig. 1a) without TBHA treatment and the other treated with TBHA 1% solution (Fig. 1b). The layer without TBHA treatment shows pores filled with tin oxide but not completely, leaving empty spaces inside the pore, whereas a thick tin oxide crystallized on the surface can be observed. This suggests rapid oxide crystallization at the top of the pores, inhibiting the entrance for the rest of the material deposited into pore depth. The hydrophobicity of PS structures after the anodization process [15] can be the main cause for this behavior. In order to avoid this problem, we functionalized the porous layers dipping them in a TBHA solution 1% to obtain the polar group ($^-$OH) adsorbed on the pore walls. Treated samples with this modification process allowed a bigger proportion of SnO_2:F to penetrate into the porous structure (Fig. 1b), leading to a more efficient filling of the pore.

It is believed that the functionalization process produces Si–$(OH)_x$, and Si–O [19,20] terminators that favors the tin oxide deposition.

We performed infrared spectroscopy on the samples to confirm the pore wall functionalization with $^-$OH groups. Fig. 2 presents infrared transmittance spectra of the same sample before and after TBHA surface treatment. It can be seen the modification introduced by the use of this compound over the PS layers for a given concentration. In order to highlight the effects introduced by the TBHA, each spectrum shown in this figure has been obtained using different references. The spectrum of the PS sample without functionalization treatment is referred to a plane silicon wafer, while the spectrum corresponding to the functionalized sample is referred to a PS sample. The presence of Si–O–Si antisymmetric stretching about 1050 cm^{-1} and the O–H stretching of $Si(OH)_x$ in 3550 cm^{-1} after the TBHA treatments indicates that the surface acquires a hydrophilic character, enabling the tin oxide precursor to penetrate the porous structure. Moreover, the mirror peaks observed in the TBHA treated sample

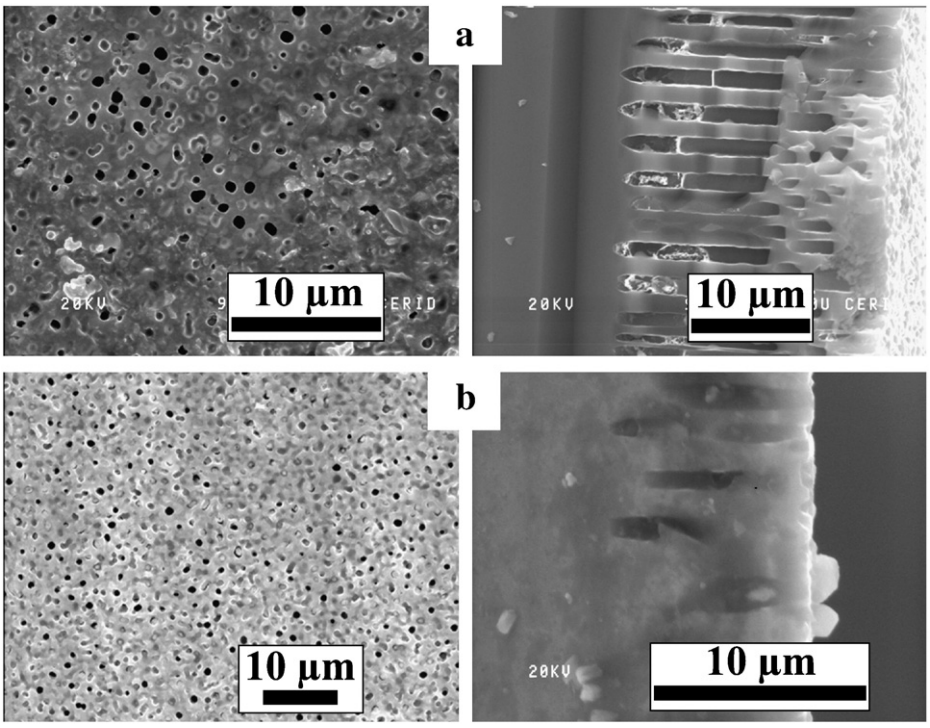

Fig. 1. SEM images of SnO_2:F coated on macroporous silicon layers (a) without TBHA and (b) with TBHA 1% for10 min in an ultrasonic bath.

Author's personal copy

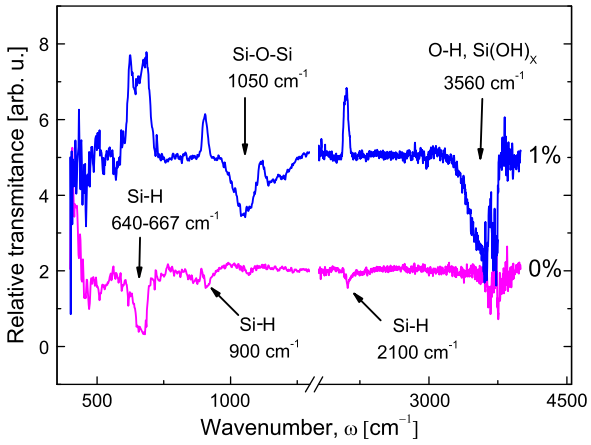

Fig. 2. Infrared spectra of samples without TBHA (0%) and with TBHA (1%) treatment. One of the spectrums has been shifted in the vertical direction for the sake of clarity. PS with TBHA was measured using as reference the PS without TBHA, and this in turn was referred to a crystalline silicon substrate. The positives peaks (640–667, 900 and 2100 cm^{-1}) correspond to the liberation of hydrogen.

(640–667, 900 and 2100 cm^{-1}) indicate that hydrogen is removed from the PS surface as the functionalization process take place.

Fig. 3 shows the X-ray diffraction spectra for SnO_2:F/PS layers with different fluorine doping concentration in the precursor solution. There is an intense peak (PS) about 32.5°, which is attributed to PS substrates [21]. This has been subtracted for better comparison. The SnO_2 contribution corresponds to polycrystalline film with a prominent peak in the (110) orientation. The angles' positions for the other planes as well as their relative intensities are in good accordance with the patterns of cassiterite phase (reference 1-072-1147 reported in the ICSD database), denoting the existence of the tetragonal phase of SnO_2 with no preferential orientations. The spectra also show peaks (labeled with asterisks in Fig. 3) that may correspond to complex silicate formation [22].

Although PS is grown from a single Si crystal substrate with (100) orientation, some peaks observed in the X-ray spectra do not correspond with this orientation. This phenomenon has been reported previously and it is attributed to different causes: PS oxidation [23,24], anodized process [25], microcrystal distortion [26] and to a micropore random distribution [27]. They have been labeled as "PS" in Fig. 3.

The vertical dashed lines superimposed to the X-ray spectra in Fig. 3 indicate the expected position for the most intense peaks of

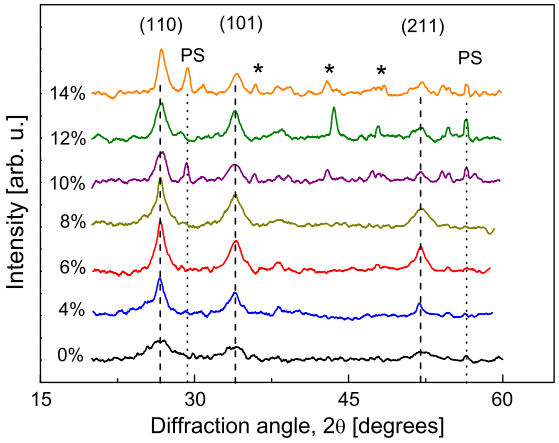

Fig. 3. X ray diffractions patterns of SnO_2:F/PS for different concentrations of NH_4F, as indicated in the figure. Vertical dashed lines indicate the pattern of SnO_2 for all orientations, the dotted lines (PS) correspond to orientations of PS substrate and dotted lines (*) indicate the diffraction peak positions for complex silicate.

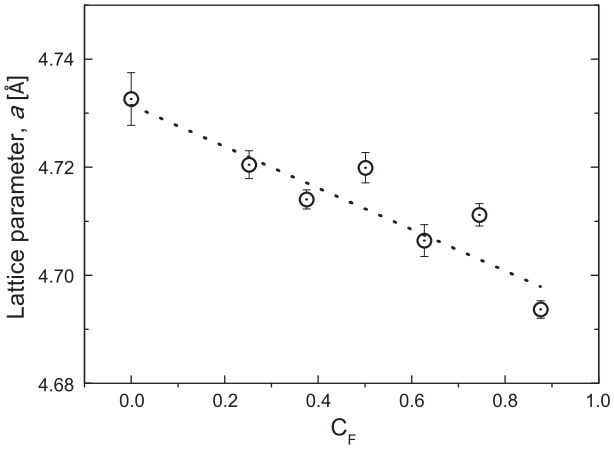

Fig. 4. Lattice parameter a as a function of fluorine concentration calculated from data of X-ray diffraction in Fig. 3. The dotted line is drawn to aid the eyes.

SnO_2 crystallized in the tetragonal structure. From Fig. 3 it has been detected a shift of the two major peaks of the SnO_2 structure to higher diffraction angles as the fluorine content increases in the samples. In order to measure the shift, the (110) and the (101) peaks were fitted with a Gaussian curve. The position of both peaks is used to determine the lattice constants. The observed shift is indicative of a change in the lattice parameters. The shift may be accounted by a decrease of the lattice parameter a, keeping the relation $a = b$, while c remains constant (see Fig. 4). Even when the ionic radii of the F (1.36 Å) is not too different from the O ionic radii (1.40 Å), there has been previous reports in other material where the partial replacement of oxygen by fluorine produces similar results [28,29].

$$C_F = \frac{n(NH_4F)}{n(SnCl_4 \cdot 5H_2O)}, \tag{1}$$

Whenever we refer to fluorine concentration in this work, we mean the number resulting from Eq. (1) [8].

In Eq. (1), $n(NH_4F)$ and $n(SnCl_4 \cdot 5H_2O)$ correspond to moles of ammonium fluorine and moles of tin chloride in the solution, respectively. The explored concentration range corresponds to fluorine/tin relation that goes from 0 to 0.9 fluorine atoms for each tin atom in the solution. Note that this ratio exists in the precursor solution, and not necessarily in the deposited film.

An estimation of the grain size is possible from the X-ray spectra of Fig. 3 by using the Scherrer's formula [30]:

$$D = \frac{0.9\lambda}{\beta \cos\theta}, \tag{2}$$

where λ is the X-ray's wavelength (0.154 nm in this case), β is the peak width at half-maximum (in radians) and θ is the angle of the corresponding peak. A large-grained polycrystalline sample was used as a reference for the determination of the instrumental broadening. The crystallite size is obtained considering the FWHM (Full Width Half Maximum) of the (110) and the (101) peaks. The peaks were fitted by a Gaussian. The FWHM values, and their corresponding errors, are presented in Table 1. The sizes calculated from the two peaks using Eq. (2) are averaged in order to get the final size. The error bars correspond to the standard deviation resulting from this average.

The results are presented in Fig. 5 where the grain size is shown as a function of fluorine concentration. The calculations yield a grain size in the range of 4–12 nm as the fluorine atoms proportion varies from 0 to 0.9 in tin oxide structure, respectively. Previous publications reported on films deposited onto flat substrates, show that these

Author's personal copy

Table 1
FWHM values, with the corresponding errors, for peaks (110) and (101).

C_F (%)	FWHM (°) (110)	Error	FWHM (°) (101)	Error
0	2.078	0.0397	1.510	0.0493
4	1.133	0.0258	1.060	0.0400
6	0.915	0.0180	1.063	0.0250
8	0.952	0.0107	1.260	0.0217
10	0.906	0.0210	0.975	0.0448
12	0.914	0.0180	0.892	0.0346
14	0.736	0.0154	0.932	0.0224

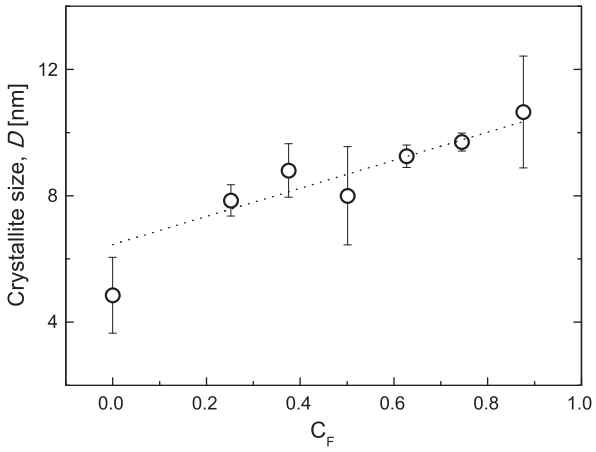

Fig. 5. Crystallite size as a function of fluorine concentration obtained using the Scherrer's formula and the data obtained of the full width at half-maximum in each diffraction peak of Fig. 3. The dotted line is drawn to aid the eyes.

films could growth in an epitaxial way, allowing sizes between 30 and 40 nm [8,9]. In our layer, the crystallite sizes are half of those reported previously. It could be attributed to the fact that the substrates utilized in this work are porous layers. It is expected a large number of nucleation sites on the surface of the pores due to defects that occur along this surface. The large number of nucleation sites may lead to smaller crystal sizes than previous reports. Additionally, we can observe an appreciable change in the crystallite size as the fluorine concentration increases indicating that F doping caused the degree of crystallinity of the SnO_2 films to increase. A similar behavior has been observed in Ref. [9] for SnO_2:F films deposited on flat surfaces.

A scheme of the tin oxide structure is shown in Fig. 6.

This compound has a tetragonal lattice with two molecules per unit cell; it has also a spatial group $P4_2/mnm$, with four oxygen atoms and two tin atoms per unit cell. The positions in the unit cell for the tin atoms are (0, 0, 0) and (1/2, 1/2, 1/2) and the oxygen atoms are at $\pm(u,u,0)$ and $\pm(u+1/2, 1/2\text{-}u, 1/2)$, where $u=0.307$ [8].

The fluorine incorporation was simulated using three different options. These options are: I — substitutional replacement of oxygen, II — F being located on interstitial sites such as (1/2, 0, 1/2), (0, 1/2, 1/2), and III — the two events (I and II) occur simultaneously with the same probability.

Considering the above information and using the prominent peaks for the rutile structure in the directions (110), (101), (200) and (211), it is possible to compute the structure factor $F(hkl)$ as [31,32]

$$F(hkl)_{SnO_2} = \sum_{i}^{unit\_cell} f_i O_i \exp\left(\frac{B_i \sin^2\theta}{\lambda^2}\right) \times \exp|2\pi i(hx_i + ky_i + lz_i)|, \quad (3)$$

where i represents Sn, F and O atoms, f_i is the atomic form factors for the three atoms in the unit cell, and B_i corresponds to the Debye-Waller correction factor due to thermal vibrations [26]. For the atomic form factor we used the coefficients tabulated for Sn, O and F in Ref. [33]. We use the B_i factor reported to be 0.04 Å for SnO_2 [34]. The occupation probability for each atom in the unit cell O_i introduces a notion of the substitution or occupation for the three atoms of the unit cell for each position. Finally, hkl corresponds to diffraction directions for each plane of interest in the unit cell. The calculation of the structure factor allows evaluating the trend in the X-ray spectra with increasing fluorine concentration. The factor is calculated taking into account the three possible localizations mentioned, for the doping atom. We calculate the ratio of the structure factors of the measured main peaks ((101) and (110)). The relationship between other peaks does not provide major information, because the error bars for these relationships are too large, giving in consequence no further information.

It is possible to observe in Fig. 7 the peak's relation for the three possibilities considered for the fluorine location in the tin oxide structure. These show a linear trend with different slopes, when plotted as a function of the fluorine concentration. The variation of the intensity ratio, $F(101)/F(110)$, measured as a function of the doping level is compared to the theoretical computed results. The resulting ratios show a small negative slope as a function of fluorine concentration.

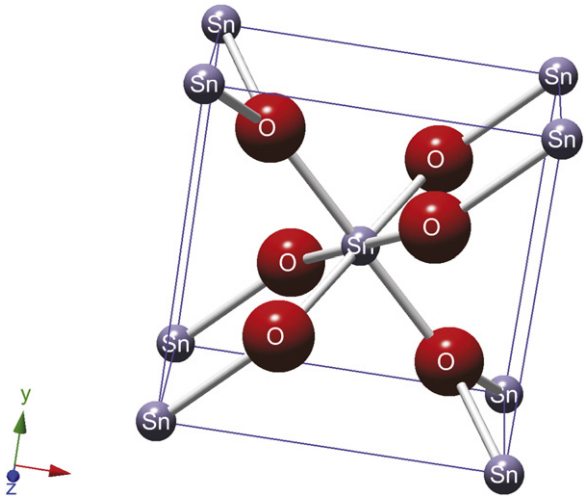

Fig. 6. Scheme of the tin oxide structure unit cell. The larger spheres (O) represent the oxygen atoms and the small spheres (Sn) represent the tin atoms.

Author's personal copy

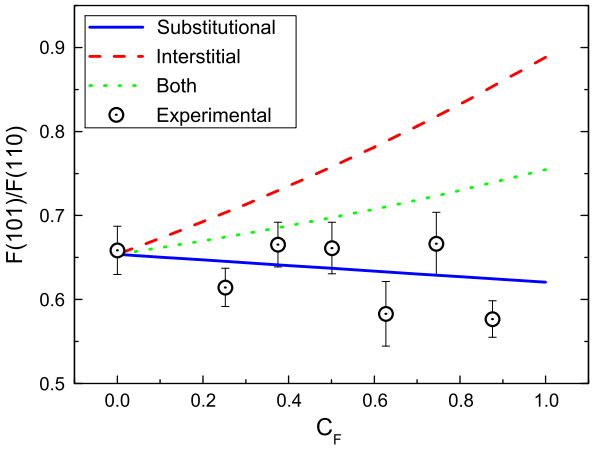

Fig. 7. Structure factor relation $F(101)/F(110)$ calculated in this work for different fluorine concentrations. Lines represent calculations made by using Eq. (3), while circles denote the structure factors taken from the measured X-ray diffraction spectra.

This slope has a similar behavior to that of the structure factor calculated for the substitutional replacement of oxygen ions by fluorine ions. Therefore, the tendency of this experimental ratio as a function of fluorine concentration shows a strong evidence that the oxygen atoms are replaced in a substitutional way by fluorine atoms. Then, fluorine ions are located in oxygen positions with increasing fluorine concentration. This result is in accordance with the dependence of lattice parameter as a function of fluorine concentration shown in Fig. 4, where we can see a decrease of this parameter as fluorine concentration increases in the solution.

4. Conclusions

The TCO/semiconductor heterostructures were obtained through sol–gel synthesis of SnO_2:F on macroporous silicon. We show that appropriated functionalization of macroporous silicon structures allow a better deposition of the tin oxide, improving the interface SnO_2:F/PS union. We found that the fluorine concentration affect the structural properties of SnO_2, by changing its lattice parameter and crystallite size. For larger fluorine concentrations, smaller lattice parameter is obtained; whereas the crystallite size increases with more fluorine atoms present as dopant. By comparing the structure factor calculations with the experimental data of X-ray spectra we demonstrate that the fluorine ions occupy substitutional sites, replacing oxygen atoms in SnO_2. This conclusion is in agreement with previous publications.

Acknowledgments

This work was partially supported by projects of the ANPCyT (PICT 32515) and by a project of Universidad Nacional del Litoral (CAID 2009 Nro 68-343). We acknowledge to R. Candal of INQUIMAE Institute of Universidad de Buenos Aires, for providing us the TBHA solutions.

References

[1] K. Daoudi, C.S. Sandu, A. Moadhen, C. Ghica, B. Canut, V.S. Teodorescu, M.G. Blanchin, J.A. Roger, M. Oueslati, B. Bessaïs, Mater. Sci. Eng. B 101 (2003) 262.
[2] A.G. Macedo, E.A. de Vaconcelos, R. Valaski, F. Muchenski, E.F. da Silva Jr., A.F. da Silva, L.S. Roman, Thin Solid Films 517 (2008) 870.
[3] E. Comini, G. Faglia, G. Sberveglieri, Sens. Actuators, B 76 (2001) 270.
[4] M.C. Esteves, D. Gouvêa, P.T.A. Sumodjo, Appl. Surf. Sci. 229 (2004) 24.
[5] A.V. Moholkar, S.M. Pawar, K.Y. Rajpure, C.H. Bhosale, J.H. Him, Appl. Surf. Sci. 255 (2009) 9358.
[6] N.G. Deshpande, J.C. Vyas, R. Sharma, Thin Solid Films 516 (2008) 8587.
[7] K.K. Purshothaman, M. Dhanashankar, G. Muralidharan, Curr. Appl. Phys. 9 (2009) 67.
[8] D. Zaouk, R. al Asmar, J. Podlecki, Y. Zaatar, A. Khoury, A. Foucaran, Microelectron. J. 38 (2007) 884.
[9] M. Oshima, K. Yoshino, J. Electron. Mater. 39 (2010) 819.
[10] O.I. Velikokhatnyi, P.N. Kumta, Phys. B 406 (2011) 471.
[11] D. Calestani, M. Zha, A. Zappettini, L. Lazzarini, G. Salviati, Mater. Sci. Eng C 25 (2005) 625.
[12] Y. Muto, N. Oka, N. Tsukamoto, Y. Iwabuchi, H. Kotsubo, Y. Shigesato, Thin Solid Films 520 (2011) 1178.
[13] E. Elangovan, M.P. Singh, K. Ramamurthi, Mater. Sci. Eng. B 113 (2004) 143.
[14] A. Moadhen, H. Elhouichet, S. Romdhane, M. Oueslati, J.A. Roger, H. Bouchriha, Semicond. Sci. Technol. 18 (2003) 703.
[15] P.G.L. Baker, R.D. Sanderson, A.M. Crouch, Thin Solid Films 515 (2007) 6691.
[16] J.N. Chazalviel, A. Belaïdi, M. safi, F. Maroun, B.H. Erné, F. Ozanam, Electrochim. Acta 45 (2000) 3205.
[17] B. Gottleb, R. Koropecki, R. Arce, R. Crisalle, J. Ferron, Thin Solid Films 13 (1991) 199.
[18] M.K. Lee, y.H. Wang, C.H. Chu, IEEE J. Quantum Electron. 33/12 (1997) 2199.
[19] L.N. Acquaroli, A. Brondino, J.A. Schmidt, R.D. Arce, R.R. Koropecki, Phys. Status Solidi C 6/7 (2009) 1546.
[20] Y.H. Ogata, T. Tsuboi, T. Sakka, S. Naito, J. Porous Mater. 7 (2000) 63.
[21] D. Bellet, G. Dolino, Phys. Rev. B 50 (1994) 17162.
[22] A.J. Locock, R.A. Ramik, M.E. Back, Can. Mineral. 44 (2006) 1457.
[23] Y.H. Ogata, N. Yoshimi, R. Yasuda, T. Tsuboi, T. Sakka, A. Otsuki, J. Appl. Phys. 90 (2001) 6487.
[24] V. Lehmann, B. Jobst, T. Muschik, A. Kux, V. Petrova-Koch, Jpn. J. Appl. Phys. 32 (1993) 2095.
[25] M. Banerjee, E. Bontempi, A.K. Tyagi, S. Basu, H. Saha, Appl. Surf. Sci. 254 (2008) 1837.
[26] A. Bensaid, G. Patrat, M. Brunel, F. de Bergevin, R. Hérino, Solid State Commun. 79 (1991) 923.
[27] M.W. Cole, J.F. Harvey, R.A. Lux, D.W. Eckart, R. Tsu, Appl. Phys. Lett. 60 (22) (1992) 2800.
[28] F. Montilla, E. Morallón, A. De Battisti, A. Benedetti, H. Yamashita, J.L. Vázquez, J. Phys. Chem. B 108 (2004) 5044.
[29] M. Kul, A.S. Aybek, E. Turan, M. Zor, S. Irmak, Sol. Energy Mater. Sol. Cells 91 (2007) 1927.
[30] P.M.R. Kumar, C.S. Kartha, K.P. Vijayakumar, T. Abe, Y. Kashiwaba, F. Singh, D.K. Avasthi, Semicond. Sci. Technol. 20 (2005) 120.
[31] R.W.G. Wyckoff, Crystal Structures Handbook, Interscience Publisher Inc., New York, 1948.
[32] M. Birkholz, P.F. Fewster, C. Genzel, Thin Film Analysis by X-ray Scattering, WILEY-VCH Verlag GmbH & Co, Weinheim, 2006.
[33] E.N. Maslen, A.G. Fox, M.A. O'Keefe, in: E. Prince (Ed.), International Tables of Crystallography, Vol. C, Kluwer Academic, Dordrecht, 2004, p. 554.
[34] G.E.S. Brito, H. Fischer, A.F. Craievich, R.R. Gonçalves, S.J.L. Ribeiro, J. Sol-Gel Sci. Technol. 28 (2003) 45.